

# Coordinated and sequential activation of neutral and acidic DNases during interdigital cell death in the embryonic limb

J. A. Montero · C. I. Lorda-Diez · A. C. Certal ·  
N. Moreno · J. Rodriguez-Leon · A. Torriglia ·  
J. M. Hurle

Published online: 8 July 2010  
© Springer Science+Business Media, LLC 2010

**Abstract** Interdigital tissue regression during embryonic development is one of the most representative model systems of morphogenetic cell death, but the degenerative cascade accounting for this process awaits clarification. Although the canonical apoptotic caspase pathway appears to be activated in the interdigital mesenchyme committed to die, neither genetic nor chemical blockage of caspases or their downstream effectors, is sufficient to prevent cell death. Hence, alternative and/or complementary dying pathways must also be responsible for this degenerative process. In this work we have chosen to study the endonucleases during the regression of the interdigital tissue of avian embryos to gain insights into the molecular mechanisms accounting for programmed cell death in this system. We show that caspase activated DNase, which is a neutral DNase associated with the caspase apoptotic pathway, appears to be the main endonuclease only at an initial phase of interdigit regression. However at peak stages of

the degenerative process, the acidic DNases L-DNase II and lysosomal DNase IIB become predominant in the system and markers for cell autophagy become moderately up-regulated. Consistent with the activation of acidic endonucleases we observed that microenvironmental pH value in the interdigits decreased to levels only appropriate for acidic enzymes. Furthermore, we found that overexpression of lysosomal DNase IIB in embryonic limb mesoderm promoted cell death, which was also accompanied by up-regulation and activation of L-DNase II. Up-regulation of acidic DNases was maintained in interdigits explanted to culture dishes, where the participation of exogenous professional phagocytes of hematopoietic origin is avoided. Finally, and consistent with all our findings, up-regulation of acidic DNases was much reduced in the webbed interdigits of duck embryos, characterized by a rudimentary interdigital degenerative process. We conclude that the regression of the interdigital tissue involves a coordinated and sequential activation of the caspase and lysosomal degenerative molecular cascades.

J. A. Montero and C. I. Lorda-Diez have contributed equally to this work.

J. A. Montero · C. I. Lorda-Diez · J. M. Hurle (✉)  
Departamento de Anatomía y Biología Celular,  
Facultad de Medicina, Universidad de Cantabria/IFIMAV,  
39011 Santander, Spain  
e-mail: hurlej@unican.es

A. C. Certal · N. Moreno  
Instituto Gulbenkian de Ciência, 2780-156 Oeiras, Portugal

J. Rodriguez-Leon  
Departamento de Anatomía, Biología Celular y Zoología,  
Universidad de Extremadura, 06006 Badajoz, Spain

A. Torriglia  
INSERM UMRS 872 eq 17, Rue de l'école de Médecine,  
75006 Paris, France

**Keywords** Apoptosis · Autophagy · LC3B · Caspases · Sequestosome · Lysosomes · Serpin B1 · Programmed cell death

## Introduction

Programmed cell death plays a crucial role during embryonic development in sculpturing the morphology or the structure of developing organs (morphogenetic and histogenetic cell death) and eliminating cells with transitory functions in the embryo (phylogenetic cell death; [1]). Interdigital cell death (ICD) is responsible for the formation of free digits in vertebrates and is among the best

characterized degenerative processes occurring in amniotic embryos (reviewed by [2, 3]). Inhibition of ICD causes syndactyly [4], and species with webbed digits, such as the duck, the turtle, or the bat, exhibit a severe diminution of ICD as compared with species with free digits such as the chick, the lizard or the human [5, 6]. ICD is TUNEL positive and is associated with internucleosomal DNA fragmentation [7]. However morphological studies reported that while the morphology of the dying cells corresponds largely with apoptosis [8], dying cells with necrotic appearance are also observed in the areas of cell death of the developing limb [9, 10].

Genetic studies in mice indicate that the mitochondrial pathway is required for interdigital cells to die, as combined knock-out of Bax and Bak [11] or Bax and Bim [12], results in syndactylous phenotype. While these factors are associated with caspase activation, Bax can function also in the cell death process involving lysosomal enzymes [13, 14] and reactive oxygen species [15].

Activation of different caspases has been detected in the interdigital dying cells [16] but neither chemical nor genetic inhibition of initiator or executioner apoptotic caspases block ICD [16–18]. Furthermore, analysis of ICD in Apaf1-deficient mice suggested the activation of a necrotic cell death mechanism in the absence of activation of caspase 9 [19, 20]. Consistent with these findings, lysosomal markers are intensely up-regulated in the interdigital mesenchyme committed to die [18, 21] and combined chemical inhibition of caspases and cathepsin D is followed by intense inhibition of the degenerative process [18]. Oxidative stress has also been implicated as a triggering factor for ICD [22, 23], and the mitochondrial apoptotic inducing factor (AIF) undergoes nuclear translocation in the course of interdigital tissue degeneration [16]. Altogether these findings suggest that either ICD involves more than one death mechanism or alternatively that when the canonical apoptotic pathway is inhibited, a secondary lysosomal pathway is activated.

Endonucleases are final effectors of dying processes responsible for DNA degradation. In the canonical caspase-mediated cell death pathway, caspase 3 cleaves a cytoplasmic heterodimeric protein, first designated DNA fragmentation factor (DFF), to generate an active neutral endonuclease caspase-activated DNase (CAD) which translocates into the nucleus to fragment DNA at the internucleosomal regions [24]. Other neutral endonucleases are also involved in apoptotic processes, such as the Granzyme A-activated DNase (GAAD) or the endonuclease G (see [25]). In contrast to neutral endonucleases, acidic cytoplasmic endonucleases are major effectors of necrotic processes while in physiological cell death they are thought to be responsible for the degradation of the DNA of the apoptotic cells engulfed by macrophages

[20, 26–28]. Taking into account that both caspases and lysosomal cathepsins appear to contribute to cell death during ICD, in this work we have chosen to study the endonucleases to gain insights into the molecular mechanisms underlying this physiological degenerative process. Our hypothesis was that the confluence of more than one death signaling pathway in ICD would be reflected in a differential implication of neutral and acidic DNases. Our findings are consistent with ICD taking place in two successive steps: the first involving caspases and CAD, and the second characterized by the incorporation of lysosomal DNase IIB and the acidic L-DNase II produced by cleavage of Serpin B1 leukocyte elastase inhibitor (LEI). We further show that such coordinated involvement of distinct cell death pathways in the course of interdigital tissue regression reflects an adaptation of the degenerative cell machinery of the embryonic limb mesenchyme to intracellular and extracellular pH acidification, that occurs with the progress of the degenerative events initiated by the canonical caspase pathway.

## Materials and methods

### Animal models

Our lab has largely used avian embryos to study different developmental processes in vertebrates [16, 29, 30]. In this work, we employed Rhode Island chicken embryos from day 5 to day 10 of incubation (id) equivalent to stages 28–36 [31] and Royal Pekin duck embryos from 8 to 11 days of incubation.

### Morphology of the regressing interdigits

The morphology of the interdigital tissue was studied in histological sections of samples fixed in 4% paraformaldehyde and embedded in araldite and by scanning electron microscopy in specimens fixed in 4% glutaraldehyde.

Antibodies, immunolabeling, TUNEL assay, and confocal microscopy

Polyclonal rabbit antibodies were employed to detect Serpin B1 [32], DNase IIB (Abnova) and LC3B (cell signaling). Monoclonal antibodies from the Developmental Studies Hybridoma Bank were also used against lysosomes (LEP100) and macrophages (TAP1). For immunolabeling, samples were fixed in 4% paraformaldehyde except for immunolabeling for DNaseIIB, which was better detected following fixation in Bouin's fluid. Most samples were used for double labeling with the TUNEL method. Details for staining procedures have been described previously

[16]. Samples were examined with a laser confocal microscope (LEICA LSM 510) by using a Plan-Neofluar 10×, 20× or Plan-Apochromat 63× objectives, and an argon ion laser (488 nm) to excite FITC fluorescence and a HeNe laser (543 nm) to excite Texas Red.

#### Overexpression experiments

For functional experiments we employed constructs containing the full-length of the human *DNase IIB* gene cloned into the pCX-GFP vector (pCX-endonuclease IIB-GFP; kindly provided by Hans H Chen [33]) and porcine *Serpin B1* gene cloned into The pCDNA3-1/NTGFP topo (pGFP-Serpin B1; [34]). Undifferentiated distal mesodermal cells obtained from limb buds at 5 id were electroporated by using cell nucleofector kit (Lonza) following manufacturer instructions. Control nucleofections using pCX-GFP or pCDNA3-1/NTGFP topo vectors were performed in all experiments. Nucleofected cells were cultured in DMEM (GIBCO) supplemented with 1% L-glutamine (Cambrex), 2% chicken serum (Sigma), 10% fetal bovine serum (GIBCO) and 1% PenStrep antibiotic (Sigma). The intensity of cell death in control and experimental cultures was analyzed by flow cytometry after 24, 48 and 72 h of culture. For this purpose samples containing 1 million of dissociated cells were incubated overnight at 4°C with 0.1% sodium citrate, 0.01% Triton X-100 and 0.1 mg/ml propidium iodide and subjected to flow cytometry analysis in a Becton–Dickinson FacsCalibur cytometer and analyzed with Cell Quest software.

#### In situ hybridization

In situ hybridization was performed in 100 μm vibratome longitudinal sections of autopods fixed in 4% paraformaldehyde. Samples were treated with 10 μg/ml of proteinase K for 20–30 min at 20°C. Hybridization with digoxigenin labeled antisense RNA probes was performed at 68°C. Alkaline phosphatase-conjugated anti-digoxigenin antibody (dilution 1:2,000) was used (Roche). Reactions were developed with BCIP/NBT substrate (Roche). Probes for Caspase 3, CAD, Endonuclease IIB, Serpin B1 were obtained by PCR (primers provided upon request).

#### Real time quantitative PCR for gene expression analysis

In each experiment total RNA was extracted and cleaned from specimens using the RNeasy Mini Kit (Qiagen). RNA samples were quantified using a spectrophotometer (Nanodrop Technologies ND-1000). First-strand cDNA was synthesized by RT-PCR using random hexamers, the M-MuLV

reverse transcriptase (Fermentas). The cDNA concentration was measured in a spectrophotometer (Nanodrop Technologies ND-1000) and adjusted to 0.5 μg/μl. Quantitative PCR (Q-PCR) was performed using the Mx3005P system (Stratagene) with automation attachment. In this work, we have used SYBRGreen (Takara) based Q-PCR. *Gapdh* or *Rpl13* were chosen as the normalizers in our experiments. Mean values for fold changes were calculated for each gene. Expression level was evaluated relative to a calibrator according to the  $2^{-(\Delta\Delta Ct)}$  equation [35]. Each value in this work represents the mean  $\pm$  SEM of at least three independent samples obtained under the same conditions. Samples consisted of 12 interdigital spaces. Data were analyzed using one-way ANOVA followed by Bonferroni tests for post hoc comparisons, and Student *t* test for gene expression levels in over-expression experiments. Statistical significance was set at  $p < 0.05$ . All the analyses were done using SPSS for Windows version 15.0. Primers for Q-PCR were: Chick Caspase 3: 5'-aagatggaccacgctcagg-3' and 5'-caggcagaatccagagtcc-3'; Duck Caspase 3: 5'-ggtgttgagcgacacagtg-3' and 5'-ttccgccaggagtaatagcc-3'; Chick CAD: 5'-cttcagcactggaatctcg-3' and 5'-cagttcactctctccatctcg-3'; Chick DNase IIB: 5'-gccactgaattccacctcc-3' and 5'-caggtccactgaactctctcc-3'; Duck DNase IIB: 5'-cggccatctgcataacc-3' and 5'-cggttggaaggtatcagg-3'; Chick Serpin B1: 5'-atcagctatggcttgttg-3' and 5'-cttctgtgcctctctctg-3'; Chick LC3B: 5'-caagttcctggtgccagatcacg-3' and 5'-acgtccacatgctgtg-3'; and Chick p62: 5'-gcagagcagatacaagatgg-3' and 5'-ctgacgaactgcttgactcg-3'.

#### Lysosomal stability assessment

Mesenchymal cells obtained from the third interdigit of embryonic chick at days 6 and 8 of incubation were assessed for lysosomal stability using the acridine orange (AO) uptake method. Interdigits were washed, cells resuspended in 2.5 ml complete culture medium with 10 mM HEPES supplemented with 5 μg/ml AO, incubated at 37°C for 15 min and washed in PBS. Interdigital cells were squashed in a coverslip and observed under the confocal microscope. When in neutral pH, acridine orange is hydrophobic, however in acidic conditions it is protonated what makes it cationic, preventing it from passing through the hydrophobic layers of the biological membranes. Thus AO can enter membranous organelles easily, but when content of the organelle is acidic as is the case for lysosomes, it will be trapped within the organelle. In this regard, acridine orange functions as a specific fluorescent label for lysosomes. AO is a metachromatic fluorophore as well. If excited by blue light (relocation method), it shows red fluorescence at high concentrations (lysosomal) and green fluorescence at low concentrations (nuclear and cytosolic). If, however, green excitation light is used

(uptake method), only concentrated (lysosomal) AO provide red/orange fluorescence. Rupture of initially AO-loaded lysosomes may be monitored as an increase in cytoplasmic diffuse green, or a decrease in granular red, fluorescence.

#### Extracellular pH imaging and quantification

6.5 id and 8 id chicken hindlimb autopods were pressure-microinjected in the interdigit with 0.35 mM SNARF-1 Dextran (70 KDa, Invitrogen) and subsequently mounted in a Nunc 8-well plate Ref. 155409 in PBS, pH 7.4. Images were taken in a Zeiss 510 using a 10× objective 0.3 NA. The laser excitation line was 543 nm and emission filters where 590/50IR and 680/60IR. The microscope was inside an incubator at 37°C and 5% CO<sub>2</sub> with saturated humidity. The final dye concentration in the tissue was estimated as 0.1–1 μM and calibration curves were obtained in PBS buffered at pH 6, 7 and 8. Image ratio of SNARF-1 Dextran was performed to abolish volumetric and dye asymmetries.

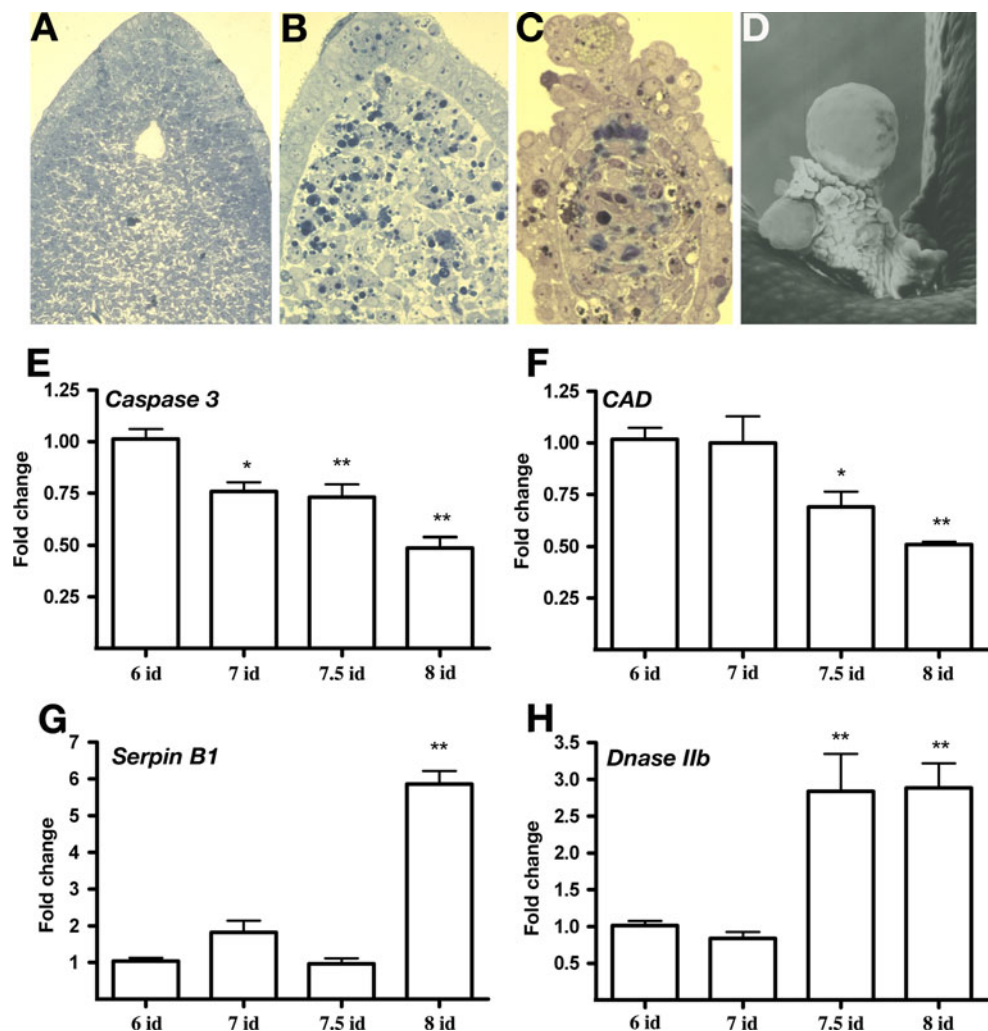
In order to produce higher intensities with lower pH, shorter wavelength was used as numerator. Image gaussing filtering and division was performed using ImageJ as  $I(590) \times 255/I(680)$  after conversion to 16 bit. Quantification was done on both emissions, average pixel intensity was measured for all interdigits and the pH estimated from the calibration curves.

#### Results

##### Morphological events in the course of interdigital cell death in the embryonic chick leg bud

Three distinctive structural stages can be identified in the course of interdigital tissue regression of the avian leg bud (Fig. 1). Prior to day 6 of incubation (6 id) the interdigits consist of a core of healthy mesenchymal cells covered by the ectoderm (Fig. 1a). Between 6.5 and 8 id, an increasing number of isolated or phagocytosed dead cells are present

**Fig. 1** Gene expression during interdigital tissue degeneration. **a–c** Longitudinal semithin sections of the third interdigital tissue during the degenerative process showing the core of mesenchymal tissue covered by ectoderm at 6 id (**a**), 7.5 id (**b**) and 8 id (**c**). Note the progressive structural alterations at 7.5 and 8 id. **d** Scanning microscopy image showing tissue detachment at the level of the third interdigital tissue at 9 id. **e–h** Scale bar diagrams showing the expression level of *Caspase3* **e**, *CAD* **f**, *Serpin B1* **g** and *DNase IIB* **h** genes during the interdigital tissue regression process. \*  $p$  value  $\leq 0.05$  or \*\*  $p$  value  $\leq 0.01$  using 6 id expression level as calibrator



in the mesenchymal core of the interdigit (Fig. 1b). From day 8 up to day 9.5 id the interdigit undergoes progressive disintegration, which includes the accumulation of dying and phagocytosed dead cells intermingled with large deposits of extracellular matrix, accompanied by the detachment of tissue clumps into the amniotic sac (Fig. 1c, d).

#### Sequential changes in caspase 3 and endonuclease gene expression during interdigital cell death

The regulation of gene expression in the course of programmed cell death has not received much attention since it has been considered that cells constitutively express the apoptotic machinery [36]. However, transcriptional regulation was observed in dying processes involving more than one lethal signaling pathway [37]. Here we choose real time Q-PCR analysis as an initial approach to investigate the involvement of caspase 3 and the different endonucleases in the course of interdigital tissue regression. Our first observation was that intensity of *caspase 3* gene expression in the interdigit showed an inverse relation with the intensity of cell death (Fig. 1e). The maximum level of expression was observed at 6 id, just preceding the initiation of the death process. In the following stages, expression was significantly reduced, and by 8 id expression reached its lowest level during the studied period. Expression of the CAD also underwent progressive down-regulation in the course of interdigit regression, reaching a significant reduction in the expression level by 7.5 and 8 id (Fig. 1f). In contrast to these genes of the canonical apoptotic pathway, we found that cytoplasmic DNases became up-regulated in the course of the regression process. Thus, *Serpin B1*, which encodes for the precursor of the L-DNase II (see [38]), was expressed at low levels in the interdigital mesenchyme prior to, and at the beginning of cell death, but underwent intense up-regulation at 8 id coinciding with the peak intensity of the death process (Fig. 1g). Transcripts of lysosomal *DNase IIB* were relatively low prior to the onset, and even at the beginning of the cell death process, but from 7.5 id, when cell death reached peak levels of intensity, the gene became intensely upregulated (Fig. 1h). These changes were not observed in samples of undifferentiated mesenchyme obtained from the distal tip of the growing digits (not shown), ruling out the possibility that the increased gene expression was associated with the maturation of the mesenchyme rather than with the progress of the degenerative process.

To further analyze the relative importance of the changes in gene regulation described above, we compared the total amount of transcripts of the studied genes in relation with expression of *Serpin B1* at 6 id, which was the gene showing the lowest level of expression during the whole

degenerative process. As shown in Fig. 2a, transcripts of CAD were predominant in the interdigits at the initiation of cell death, but the lysosomal *DNase IIB* became the predominant nuclease when cell death reached maximum intensity. Analysis of gene expression by in situ hybridization was consistent with these findings. Until 7 id, all the studied genes exhibited a homogenous pattern of expression in the autopod lacking specific domains (not shown). However, from 7.5 id the lysosomal *DNase IIB* gene exhibited an intense expression domain restricted to the interdigital tissue in the course of degeneration (Fig. 2b, c).

#### L-DNase II and DNase IIB contribute to DNA degradation in the interdigital dying cells

Since the expression of the genes encoding for cytoplasmic DNases might not necessarily reflect the presence of active enzymes playing a role in cell death, we next used immunohistochemistry to analyze the distribution of the active enzymes in the interdigital tissue. We distinguished between activity in the resident mesenchymal cells

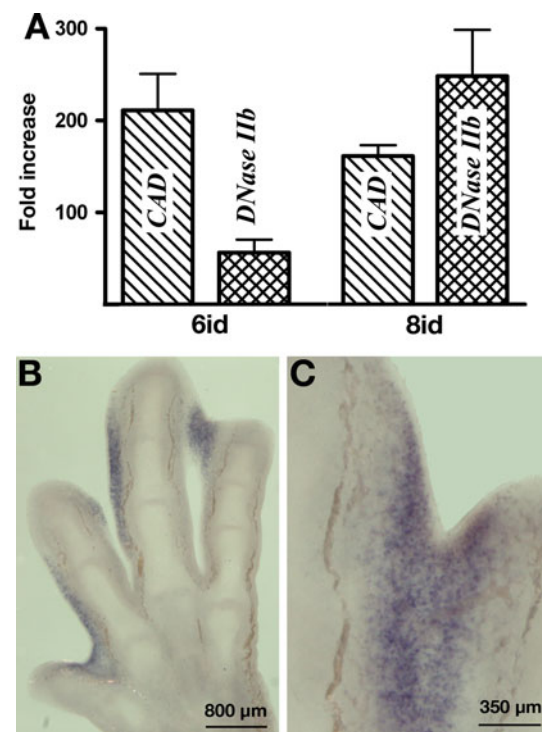
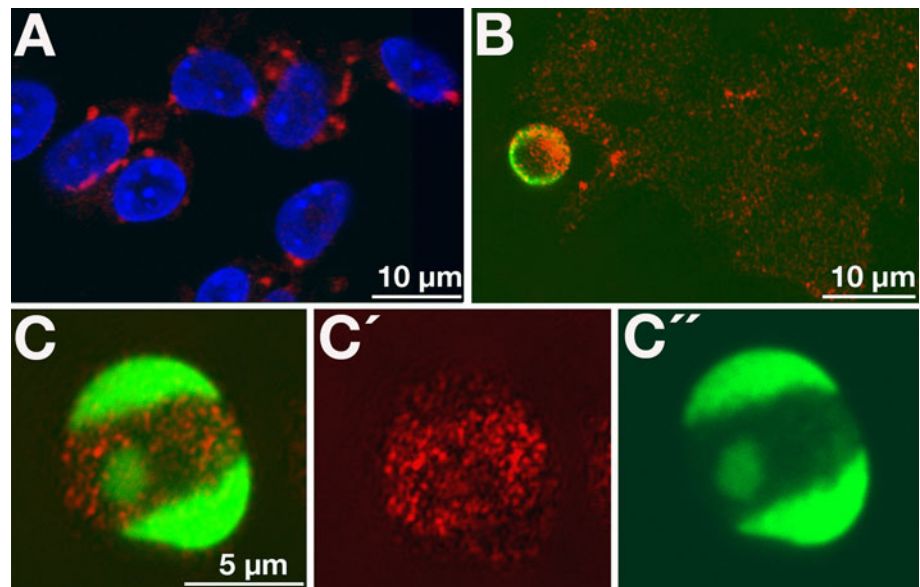


**Fig. 2** *DNase IIB* becomes the main DNase as interdigital regression progresses. **a** Expression levels of caspase activated DNase (CAD) and the acidic DNase IIB at 6 id and 8 id illustrating the increase in the expression of DNase IIB reaching the highest levels of expression by 8 id. In the scale bar diagram *Serpin B1* expression level at 6 id (not represented) was used as calibrator. **b** In situ hybridization of 8.5 id autopod showing interdigital expression of *DNase IIB*. **c** Detailed view of the third interdigit at 8 id

**Fig. 3** L-DNase II is found active in apoptotic cells. **a** Characteristic dotted L-DNase II labeling (red) in healthy mesenchymal cells from 6 id interdigit stained with DAPI (blue). **b** Interdigital mesenchymal cells from 8 id embryos where an apoptotic cell (TUNEL labeling in green) can be observed with intense L-DNase II nuclear labeling (red). **c-c''** Apoptotic interdigital mesenchymal cell positive for TUNEL (green) and L-DNase II (red) labeling. **c'** and **c''** correspond with each isolated channel. (Color figure online)



undergoing cell death and the incoming macrophages, by means of the specific macrophage antibody TAP-1 [39].

Serpin B1 is a member of the Serpin (serine protease inhibitor) superfamily, which is also known as leukocyte elastase inhibitor [40]. When apoptosis is induced under specific conditions, LEI is transformed into L-DNase II, a molecule with endonuclease activity. In the cytoplasm, Serpin B1 stands in its native form and has an anti-protease activity, but upon Serpin cleavage it is transformed into an endonuclease that translocates into the nucleus where it becomes active [38]. At 6 id, prior to the onset of cell death, the interdigital mesenchyme exhibited intense cytoplasmic but no nuclear labeling for this component (Fig. 3a). However, from 7 id, immunolabeling was intense in the nucleus of most apoptotic cells (Fig. 3b). In a quantitative approach, at day 7.5 id we detected nuclear labeling in 47 out of 60 TUNEL positive cells (78%). As shown in Fig. 3c labeling of these cells was associated with nuclear regions negative for TUNEL labeling. Nuclear labeling in TUNEL negative cells was exceptional.

Lysosomal DNase IIB was also observed in the interdigital mesenchyme prior to and during cell death, showing a characteristic lysosomal punctate pattern (Fig. 4a, b). Immunolabeling was also constant in macrophages positive for TAP1 containing phagocytosed apoptotic bodies (Fig. 4c). Furthermore, at peak cell death stages, increased labeling for this DNase was observed in dead cells with tenuous TUNEL labeling (Fig. 4d), although some labeling was also present in dead cells displaying the characteristic TUNEL labeling of apoptotic cells (Fig. 4e). A quantitative approach performed on 60 dead cells from the third interdigit at 8 id revealed that 8 dead cells (13%) exhibited intense DNase labeling in combination with tenuous TUNEL labeling; 17 (28%) were TUNEL positive and

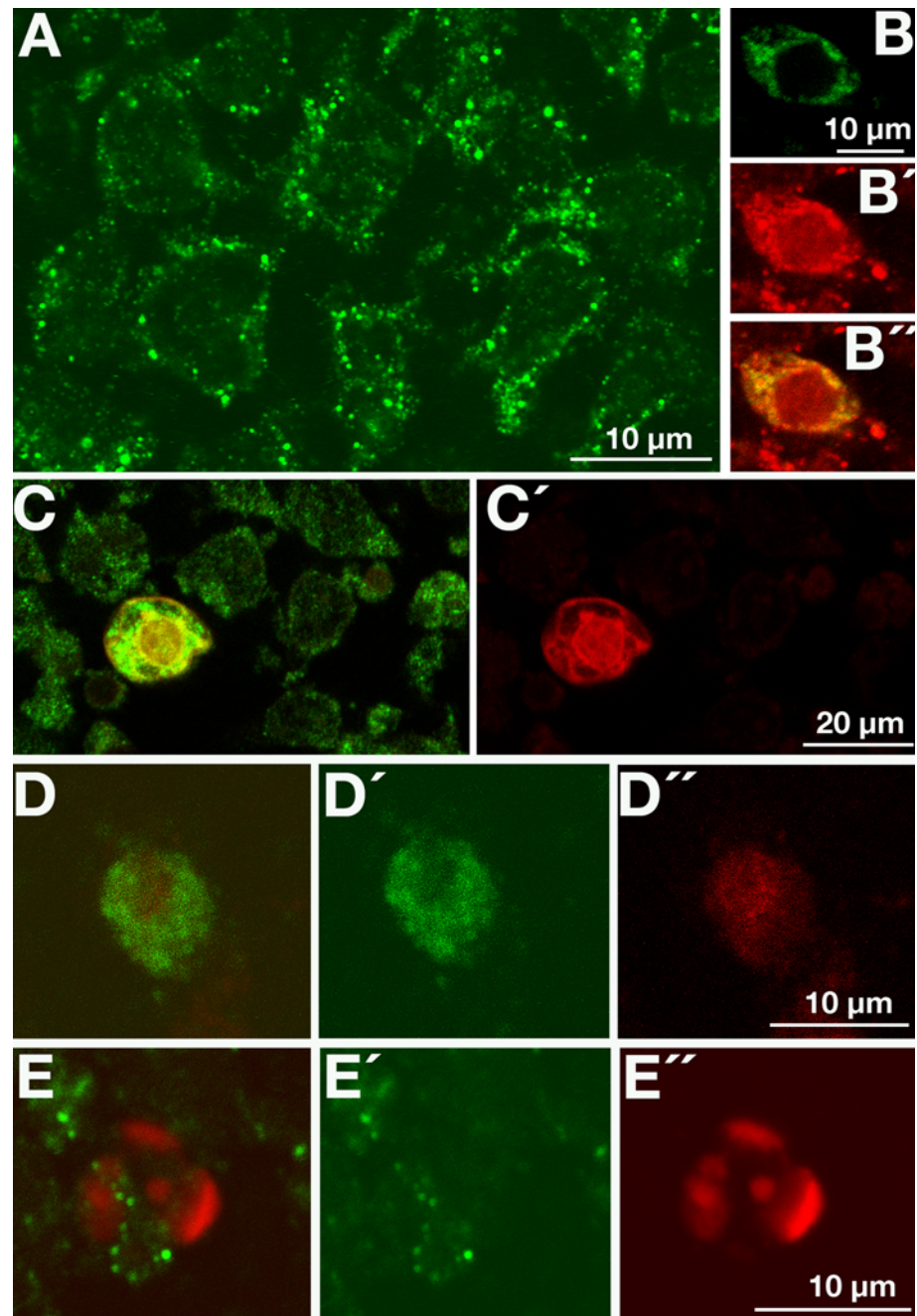
exhibited a moderate DNase nuclear labeling; and 34 (58%) were TUNEL positive but lacked nuclear DNase labeling.

#### Increased interdigital acidic DNase activity in absence of professional phagocytes

To further distinguish DNase activity of resident mesenchymal cells from that of the incoming migrating macrophages, we analyzed the distribution of acidic endonucleases in interdigital tissue explanted to organ culture at 6.5 id (just preceding the invasion of hematopoietic professional phagocytes). It has been previously established that INZ occurs according to schedule in explant cultures [41], and immunolabeling with the macrophage marker TAP1 confirmed that invading professional phagocytes are scarce in the interdigital explants (Fig. 5a, b), as could be expected by the absence of vascular blood supply. Hence, this *in vitro* approach allows a better analysis of interdigital tissue autonomous mechanisms accounting for the natural course of cell degeneration in INZ.

TUNEL analysis in tissue sections of the explants confirmed the occurrence of intense interdigital cell degeneration after 24 h of culture (not shown). Analysis of gene expression by Q-PCR showed no differences in the expression of *Caspase3* and *CAD* genes while *DNase IIB* and *Serpin B1* were significantly up-regulated (Fig. 5c). Consistent with these findings, protein expression of L-DNase II and DNase IIB was intensified in the dying interdigital mesenchyme of the explants. The pattern of immunolabeling of L-DNase II was similar to that found in *in vivo* conditions (not shown). However, immunolabeling for DNase IIB distinguished four types of dying cells

**Fig. 4** DNase IIB is found active in apoptotic cells. **a** Characteristic dotted DNase IIB labeling (*green*) in healthy mesenchymal cells from 6 id interdigit. **b–b''** Double immunolabeling for DNase IIB (*green*) and the lysosomal maker LEP100 (*red*). **b** and **b'** correspond with each isolated channel and **b''** is the merged picture. **c–c'** Double immunolabeling for DNase IIB (*green*) and the macrophage maker TAP1 (*red*). **c'** Shows only the *red* channel. **d–e''** Double TUNEL (*red*) and DNase IIB (*green*) immunolabeling of interdigital mesenchymal cells from 8 id embryo. **d** Shows a dying cell with tenuous TUNEL nuclear labeling (*red*) and intense DNase IIB labeling (*green*). **e**, Shows a TUNEL positive (*red*) apoptotic cell containing DNase IIB staining (*green*) in the nuclear regions lacking TUNEL labeling. **d'–d''** and **e'–e''** Show only the *green* and *red* channels from **d** and **e** respectively. (Color figure online)



according to their labeling pattern (Fig. 6): (i) TUNEL positive cells with DNase IIB immunolabeling in the peripheral region of the nucleus (Fig. 6a); (ii) Cells with TUNEL positive chromatin fragments intermingled with zones positive for DNase IIB labeling (Fig. 6b); (iii) Cells with tenuous TUNEL labeling also showing positive labeling for DNase IIB in the nuclear contour (Fig. 6c); and (iv) Cells TUNEL negative with very intense and diffuse cytoplasmic labeling for DNase IIB, indicative of massive lysosomal permeabilization (Fig. 6d). The first two types of cells (i, ii) are consistent with a role of the lysosomal DNases IIB in the elimination of DNA of the cells dying by

apoptosis in absence of invading macrophages. The latter two types of cells (iii, iv) are consistent with a primary role of lysosomal DNase IIB in cell death, as occurs in non-apoptotic cell death [42].

#### pH acidification in the regressing interdigits

Interdigital cell death is accompanied by important structural changes in the interdigits, including the disintegration of the blood vessels [43], that might modify the homeostatic conditions of the microenvironment of the dying cells as degeneration progresses. By monitoring cathepsin D

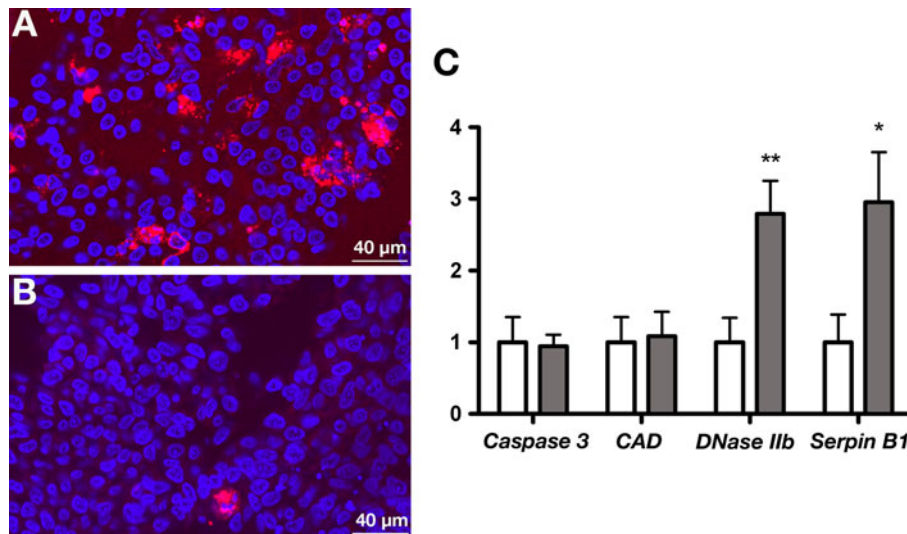


**Fig. 5** L-DNase and DNase IIB expression in cultured interdigit explants. **a–b** Interdigital mesenchymal cells from the third interdigit at 7.5 id from a control limb **a** and from an autopod explanted at 6.5 id and cultured for 24 h. Tissue was stained with DAPI (blue) and immuno-labeled with TAP1 for macrophages detection (red). Note the reduced number of macrophages in the cultured sample in comparison with their abundance in the control interdigit. **c** Diagram

showing the pattern of *Caspase 3*, *CAD*, *DNase IIB* and *Serpin B1* gene expression quantified by Q-PCR. White columns on the left illustrate the level of expression in control limbs at 6.5 id. Grey columns on the right illustrates the level of expression in cultured limbs at 6.5 id + 24 h of culture. \*  $p$  value  $\leq 0.05$  or \*\*  $p$  value  $\leq 0.01$  using expression at 6.5 id as calibrator. (Color figure online)

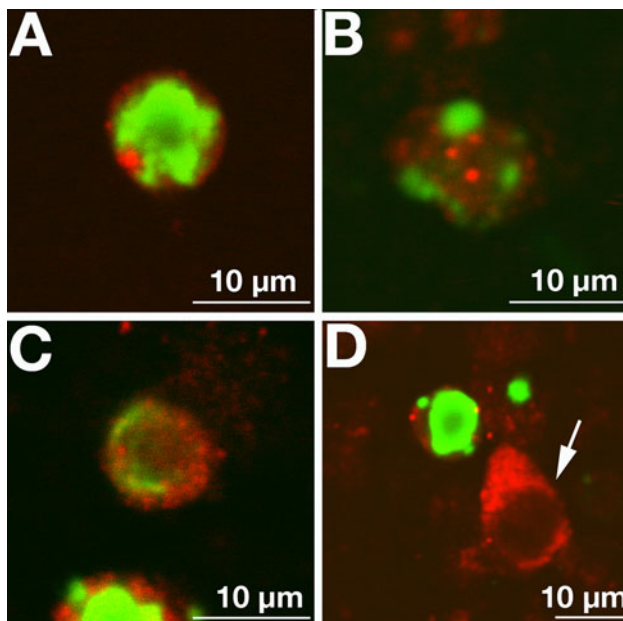


**Fig. 6** DNase IIB activity in cultured interdigit explants. **a–d** Double TUNEL (green) and DNase IIB (red) immunolabeling in interdigital cells from 6.5 id + 24 h of culture limbs. **a** Illustrates a TUNEL positive nuclei with peripheral DNase IIB positive immunolabeling. **b** Cell with TUNEL positive spots intermingled with DNase IIB staining. **c** Weak TUNEL positive nuclei with high level of DNase IIB staining. **d** TUNEL negative cell with diffuse and strong cytoplasmic DNase IIB staining (arrow). (Color figure online)

liberation and function in dying interdigital mesenchymal cells, we have previously demonstrated that lysosomes pour out their content in the course of interdigit regression [18]. To further visualize lysosomal permeabilization and intracellular acidification in the regressing interdigits, here we explored these aspects by vital staining with acridine orange (AO). We also explored extracellular acidification with Snarf1 dextran, a specific dye to evaluate extracellular pH with confocal microscopy.

AO is a lysosomotropic metachromatic fluorochrome capable of marking zones of lysosomal permeabilization characterized by an acidic pH. When excited with blue light, AO emits red–orange fluorescence at high concentration marking lysosomes, and green fluorescence at low concentrations marking the nucleus and the zones of the cytosol with acidic pH (see [13, 44]). At 7.5 and 8 id the interdigital tissue incubated for 15 min in 4  $\mu\text{g}/\text{ml}$  AO allowed us to identify (Fig. 7): (i) healthy mesenchymal cells with a characteristic red dotted staining pattern, reflecting the abundance in lysosomes in the interdigital mesenchyme at these stages (Fig. 7a); (ii) isolated rounded cells in which green staining was very intense in the cytosolic regions surrounding lysosomal aggregates stained in red, reflecting lysosomal permeabilization and cytosol acidification (Fig. 7b); and (iii) large macrophages containing vacuoles intensely stained in green or in red (Fig. 7c).



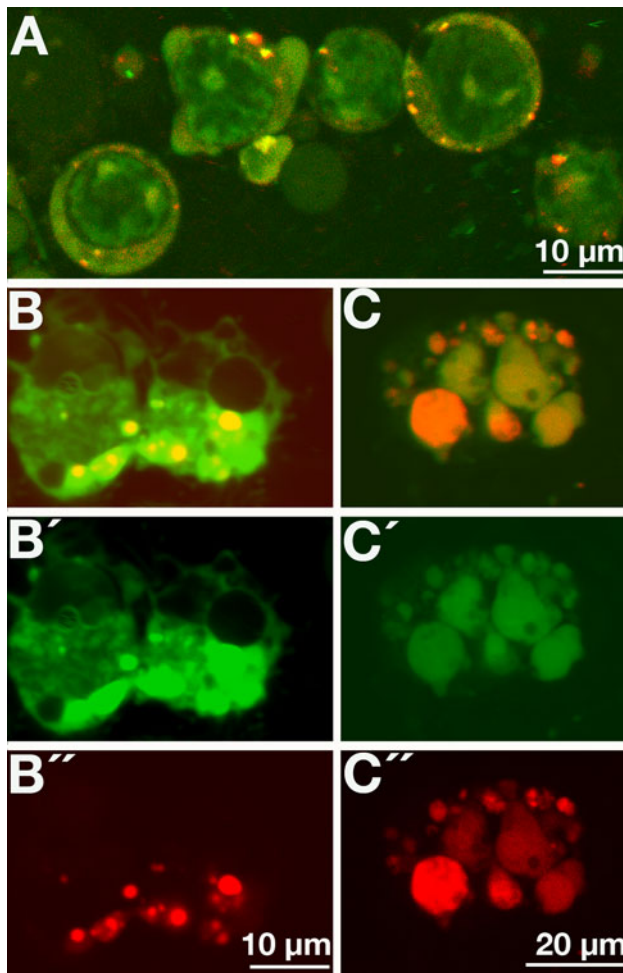


**Fig. 7** Lysosome permeabilization in interdigital cells. **a–c** Acridine orange (AO) vital staining in interdigital cells from 8 id embryos monitored by confocal microscopy. **a** This image illustrates healthy cells with green nuclei staining and dotted red/orange staining corresponding to intact lysosomes. **b–b''** Interdigital cell where a mild acidic cytoplasmic region (*green*) appears surrounding an intense acidic lysosomal region characterized by red labeling. **b'** and **b''** correspond with isolated *green* and *red* channels in **b** respectively. **c** This image illustrates the intense acridine orange staining of a macrophage with vacuoles of different acidification. **c'** and **c''** correspond with isolated *green* and *red* channels in **c** respectively. (Color figure online)

The analysis of extracellular pH was also consistent with a decrease in interdigital pH values in the course of tissue regression. As shown in Fig. 8, physiological values of pH (7.29) were measured in the interdigital tissue at 6.5 id, just preceding the onset of INZ. From this stage, pH values underwent a progressive acidification and by 8 id, interdigital pH achieved values close to 6.5.

#### Upregulation of autophagic markers in the regressing interdigits

To check whether the up-regulation of acid endonucleases in the course of interdigit regression correlates with

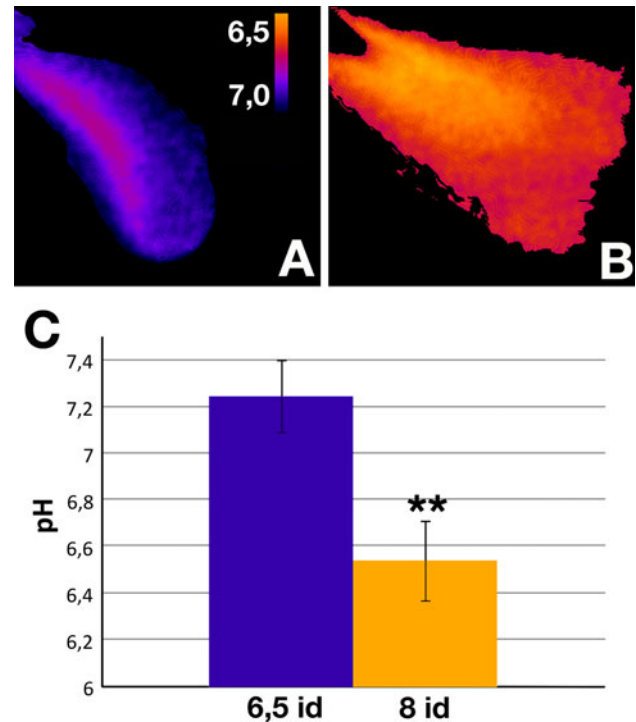


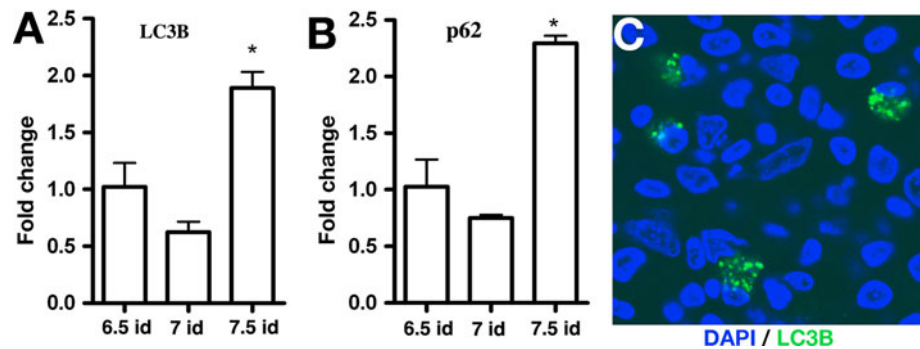
**Fig. 8** Interdigital pH acidification during tissue regression. **a, b** pH ratio imaging using SNARF-1 Dextran on 6.5 id (**a**) and 8 id (**b**). An image mask was performed to visualize only the inter-digital area. In vitro calibration was produced using the same LUT and intensity level settings for enabling directed pH level comparison. **c** Extracellular pH in chicken hindlimb interdigits. An average acidification of 0.7 pH units is observed from 6.5 id to 8 id interdigits. Error bars represent standard error.  $n = 6$  for each stage. (\*\*  $p$  value  $\leq 0.01$ )

mechanistic changes in the process of cell death, we explored the expression of LC3B (microtubule-associated protein light chain B) and p62 (sequestosome) genes as markers for autophagy (reviewed by [45, 46]). As shown in Fig. 9a, b, both genes showed a mild non-significant downregulation at the beginning of ICD, but from 7.5 id both markers became upregulated. Consistent with this finding, a moderated number of mesenchymal cells positive for LC3B immunolabeling were present in the regressing interdigits (Fig. 9c) but totally absent in non-dying regions of the autopod (i.e. forming digits). Interestingly, LC3B positive cells exhibited a preferential distribution in the proximal region of the regressing interdigits, where it has been claimed that cell death occurs under a different molecular regulation than in the distal-most interdigital mesenchyme [41].

#### Overexpression of lysosomal DNase IIB induces cell death in undifferentiated mesenchymal cells of the embryonic limb bud

To analyze the potential association of the increased expression of acidic DNases and cell death, we performed

**Fig. 9** Expression of autophagic markers in the regressing interdigit. Expression levels of *LC3B* (a) and *p62* (b) genes at 6.5, 7 and 7.5 id. (c) Immunolabeling for LC3B (green) of the proximal mesenchyme of the third interdigit at 7.5 id stained with DAPI (blue). (Color figure online)



over-expression experiments in primary cultures of embryonic limb mesenchymal cells. Undifferentiated mesenchymal cells obtained from the distal tip of limb buds at day 5.5 of incubation were nucleofected to over-express *Serp11 B1* or *DNase I1B* genes and cultured for 24, 48 or 72 h. Quantification of the number of dead cells in these cultures was performed by flow cytometry after labeling with propidium iodide. Overexpression of *Serp11 B1* gene was followed by intense cytoplasmic accumulation of the protein. Nuclear labeling was only observed in rounded cells apparently in the course of detachment into the culture medium. This indicates that, as observed in vivo, cell death in the culture conditions is accompanied by cleavage of Serpin B1 and nuclear translocation of L-DNase II. However, our findings also show that over-expression of Serpin B1 is not sufficient to induce activation of the L-DNase II. Consistent with this finding, the rate of cell death was not significantly modified in the experimental cultures (Fig. 10). In contrast, overexpression of *DNase I1B* caused an increase in cell death, which achieved significant levels by 48 h of culture (Fig. 11a). Furthermore, as observed here in the course of physiological ICD, *Serp11 B1* gene appeared intensely up-regulated (Fig. 11b) and immunolabeling for this component was seen both in the cytoplasm and in the nucleus, indicating that under these experimental conditions L-DNase II was activated. *Caspase 3* and *CAD* gene expression appeared slightly up-regulated in cells overexpressing *DNase I1B* (Fig. 11b). These findings are consistent with a cell-autonomous implication of the lysosomal DNases in programmed cell death, as observed previously in *Drosophila* [47], and support the occurrence of a crosstalk between the different degenerative routes in the course of the elimination of the embryonic limb mesodermal tissue experimentally subjected to a death signal.

Interdigital expression of *DNase I1B* gene is very low during digit formation in the webbed limb of the duck

The above described results point to lysosomal DNase I1B as a significant player in ICD at advanced stages of

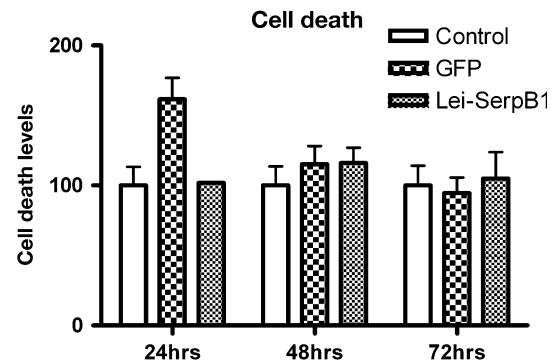


**Fig. 10** Overexpression of *Serp11 B1* is not sufficient to promote cell death. Scale bars diagram illustrating the level of cell death in mesenchymal limb cells after 24 h (left), 48 h (middle) and 72 h (right) of culture. Cell death was measured by flow cytometry in control cells (white columns on the left), cells transfected with *GFP* (middle columns) or cells transfected with *GFP-Serp11 B1* (dotted columns on the right) respectively. Cell death level in control cells is considered 100% in the diagram. No significant differences were observed in any of these days, although overexpression of *GFP* causes a moderate increase in cell death which appears attenuated in cells overexpressing *GFP-Serp11 B1*. Absence of error bars in the representation is due to presence of low values that cannot be visualized at the graph scale

interdigital tissue regression characterized by intense tissue remodeling. To further unravel the functional significance of this lysosomal enzyme, we analyzed by Q-PCR the expression of *caspase 3* and *DNase I1B* in the third interdigit of the developing leg buds of embryonic duck, as a physiological model of syndactyly (Fig. 12a). *Caspase 3* was expressed uniformly during the period covering the morphogenesis of the webbed digit of the duck. *DNase I1B* was expressed at very low levels in the interdigital tissue in comparison with expression observed in the chick (Fig. 12b). However, the increased expression pattern associated with the advanced stages of tissue regression was also maintained in the duck but such increased expression is only noted in the very late stages of digit formation (Fig. 12a). These stages are characterized by sculpturing of the distal phalanges of digit 3 and 4, which is the only portion of the digits which is free in the duck foot [48]. Analysis of the expression of L-DNase II by western

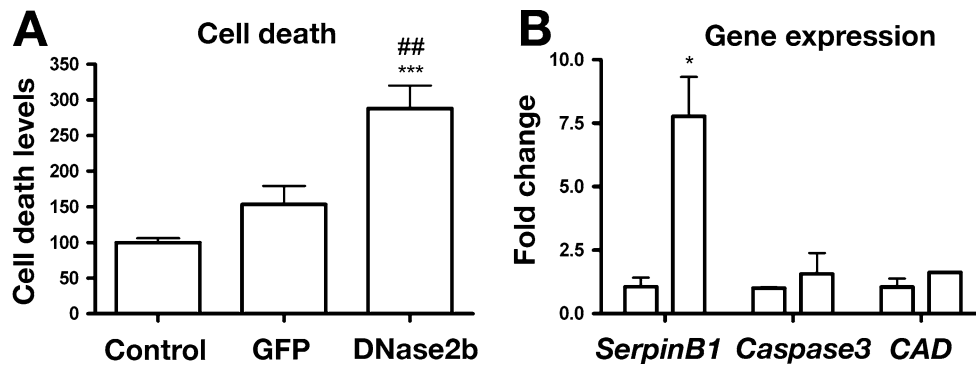


**Fig. 11** Overexpression of *DNase IIB* promotes cell death and induces the expression of *Serpin B1*. **a** Diagram illustrating the intensity of cell death in limb mesenchymal cells after 48 h of culture, as measured by flow cytometry in control cells (left), *GFP* transfected cells (middle) or *GFP-DNase IIB* transfected cells (right) respectively. Cell death in control cells is considered as 100%. ## *p* value  $\leq 0.01$  *GFP-DNase IIB* versus *GFP* cells; \*\*\* *p* value  $\leq 0.001$  *GFP-*

*DNase IIB* versus control. **b** Diagram illustrating the level of expression of *Serpin B1*, *Caspase 3* and *CAD* measured by Q-PCR in *DNase IIB* overexpressing mesenchymal cells after 48 h of culture. Expression in control cells (left column in each gene) was used as a calibrator. Note the considerable induction of *Serpin B1* expression. Absence of error bars in the representation is due to presence of low values that cannot be visualized at the graph scale. \* *p* value  $< 0.05$

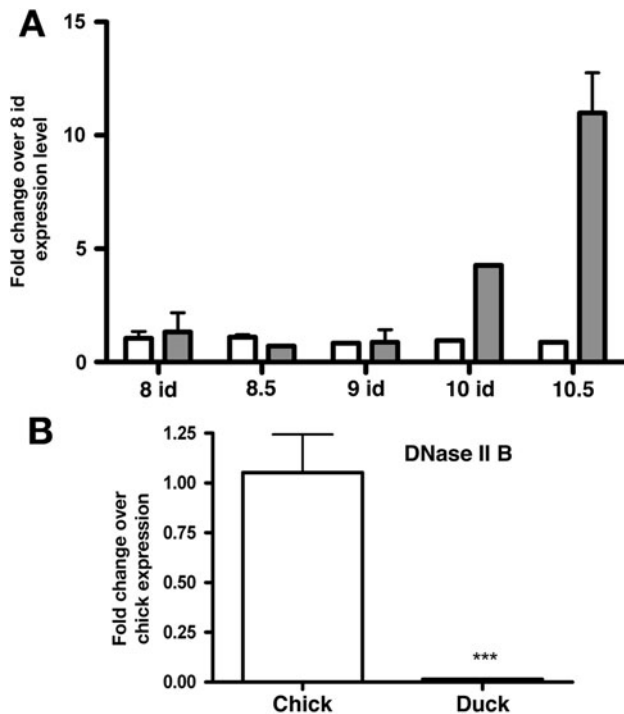


**Fig. 12** Expression of acidic DNases in the interdigital tissue of the duck. **a** Q-PCR analysis of the expression of *Caspase 3* (white bars) and *DNase IIB* (grey bars) in the interdigital tissue of the developing duck embryo at different stages of development. **b** Comparison by Q-PCR of the level of expression of *DNase IIB* in chicken (left bar) and duck (right bar) interdigital tissues at equivalent stages of development (\*\*\* *p* value  $\leq 0.001$ ). Absence of error bars in the representation is due to presence of low values that cannot be visualized at the graph scale

blot also revealed a reduced expression in the duck in comparison with expression levels in the chick (not shown). These findings indicate that the basic regression

mechanism is conserved in both species regardless of the intensity of tissue regression. However, major quantitative differences in gene regulation correlated with the reduced tissue remodeling of the webbed interdigits of the duck.

## Discussion

The areas of ICD, formerly called Interdigital Necrotic Zones, constitute one of the most illustrative examples of the role of programmed cell death in morphogenesis during embryonic development [49]. These areas, which are present in the developing limb of tetrapod vertebrates, account for digit morphogenesis. In species with free digits, ICD is very intense and sculpts the digit rays from the autopodial plate. In vertebrates with webbed digits, the intensity of cell death is reduced and most components of the interdigital mesenchyme survive [2]. In humans, abnormal inhibition of ICDs is observed in a variety of genetic diseases characterized by the formation of hands or feet with syndactyly. In chick embryos, ICD is very prominent and accounts for the full elimination of the interdigital tissue [3]. In the leg bud, the process starts by 6.5–7 id and progresses through 7.5, 8, 8.5, 9 id and by 9.5 id digits are free of each other. Two aspects are most remarkable in this process: first, it is finely regulated at both genetic and tissue levels; and second, it is not only characterized by massive mesenchymal cell death but, it is accompanied by tissue regression including the collapse of blood vessels and the disintegration of the extracellular matrix [43, 50, 51]. Here we show that these structural alterations are accompanied by acidification of the extracellular pH value, which decreases to 6.4 at 8 id when degeneration is most intense, and intracellular acidification

of the dying cells detectable by acridine orange staining. Hence, it can be expected that these changes must have a significant impact on the functional activity of the enzymatic machinery implicated in the degenerative process, including the activation of complementary or alternative routes of cell death.

The morphology of the dying cells in the areas of ICD corresponds largely with apoptosis [8, 10], and DNA degradation occurs predominantly by internucleosomal fragmentation [7]. Furthermore, caspase 9 is active in the regressing interdigits [52] and interdigital dying cells are positive for active caspase 3 and 7 immunolabeling [16, 20]. Together these findings gave an initial idea of ICD as a typical example of cell death mediated through the canonical caspase pathway. However, syndactyly was not found in knockout mice for the different apoptotic caspases, including caspase 9, caspase 8, caspase 7, caspase 6, caspase 3, and caspase 2 [17, 53, 54], or in CAD-deficient mice [26]. In addition, cell death is delayed but not inhibited in mice deficient for Apaf1, a central player in the caspase dependent apoptotic pathway and, most interestingly, the morphology of cell death in this case corresponds to necrosis rather than apoptosis [19, 20]. In accordance with these findings, we have observed previously that lysosomal cathepsins become upregulated in the course of ICD [18] and that combined treatments with caspase and cathepsin D inhibitors are more efficient in inhibiting ICD than single treatments with either caspase or cathepsin D inhibitors [18], suggesting that lysosomes are also responsible for the death process.

Our findings show that expression of *caspase 3* and *CAD* genes is highest prior to, and at the beginning of, the dying process but decreases in the course of regression suggesting that their relative contribution to the degenerative process diminishes as tissue regression progresses. In contrast, we show that expression of the acidic endonucleases are intensely up-regulated in the course of interdigital degeneration.

L-DNaseII is an acidic endonuclease produced by cleavage of Serpin B1 [25], which digests DNA giving TUNEL-negative fragments [38]. In our quantitative expression analysis, Serpin B1 gene was expressed at lower levels prior to, and at the beginning of, ICD, but showed a significant up-regulation coupled with the progress of physiological cell death both in vivo and in vitro, and also in mesenchymal cell death induced by over-expression of lysosomal DNase IIB. Furthermore, in all these situations, the up-regulation of this gene coincides with the presence of nuclear labeling in the dying cells, indicating Serpin B1 cleavage and activation of the nuclease [38]. Hence, this acidic DNase appears to be part of an enzymatic cascade regulated at transcriptional and protein level, which functions in coordination with neutral DNases to digest DNA in a cell autonomous fashion during ICD. Our functional

experiments indicate that overexpression of Serpin B1 gene is not accompanied by nuclear translocation of the DNase and increased cell death. Hence, the active involvement of this factor in ICD would require additional signals to cleave Serpin B1 and subsequent nuclear translocation of the active DNase. Consistent with the intracellular and extracellular pH modifications detected here, in the course of the degenerative process in other experimental systems Serpin B1 cleavage appears to be directed by pH acidification [55]. Interestingly, the significance of Serpin B1 in the interdigital tissue might be wider than its implication in ICD. The interdigits prior to degeneration have an elastin-rich extracellular matrix, which becomes degraded concomitantly with the progress of ICD [51]. Hence, Serpin B1, which inhibits elastase [38], might initially protect interdigital elastin from degradation and later contribute to the elimination of DNA from the dying cells.

DNase IIB is the most characteristic lysosomal endonuclease of the avian cells [56]. In mammals DNase IIA is the main lysosomal DNase and DNase IIB appears to have a limited function in the elimination of the nuclei of the differentiating lens fibers [57]. Regardless of isoform differences between species, lysosomal DNases have mainly been associated with DNA degradation by macrophages. The direct involvement of lysosomal DNases in programmed cell death has not been previously documented except for cell death in the *Drosophila melanogaster* ovary [47] and in differentiating lens fibers in the mouse eye [57]. Here we have shown that during ICD, DNase IIB is abundant not only in macrophages but also in the resident interdigital mesenchymal cells. Furthermore, we show that considerable labeling is detected in isolated dying cells, and its over-expression in limb mesenchymal cells is sufficient to promote cell death. Hence, the function of this DNase cannot be restricted to a role in the degradation of DNA by macrophages. Our analysis of gene and protein expression in cultures of interdigital tissue explanted prior to the onset of cell death, when circulating macrophages of hematopoietic origin have not yet invaded the regressing interdigits, emphasizes the importance of this enzyme in the resident interdigital mesenchyme. Previous studies have shown that interdigital mesenchyme is able to perform the function of professional phagocytes in macrophageless mouse embryos, null for the haemopoietic-lineage-specific transcription factor, PU.1 [58]. Taking all these findings together, we propose that DNase IIB will account for the degradation of DNA in the interdigital mesenchymal cells in a cell-autonomous fashion, associated with the changing microenvironmental homeostatic conditions of the regressing tissue. In addition, the enzyme will provide functional competence to interdigital mesenchyme to substitute macrophages in the elimination of DNA after phagocytic uptake of cell debris.

The activation of caspases reported in previous studies of ICD [52, 59] together with the changes in gene expression observed here during the regression of the interdigital tissue, is consistent with an initial activation of neutral endonucleases activated by caspase 3, as CAD, followed by the activation of acidic endonucleases. This interpretation correlates with the fall in the extracellular pH values of the interdigit observed in the course of tissue regression. Our results indicate that neutral (caspase-activated) and acidic DNases will be complementary and coupled degenerative players of tissue regression. The up-regulation of the autophagic markers LC3B and p62 observed here in the course of interdigit regression might suggest that the activation of the acidic endonucleases is associated with an activation of autophagy. However, cells positive for autophagic markers are not very abundant and exhibit a specific distribution in the proximal region of the interdigits. Whether autophagy is a dying mechanism characteristic of a subset of interdigital cells or if it reinforces other degenerative routes implicated in ICD awaits further analysis.

**Acknowledgments** We thank Montse Fernandez Calderón and Sonia Perez Mantecón for excellent technical assistance. This work was supported by a grant from the Spanish Education and Sciences Ministry to JMH (BFU2008-03930). CILD is a recipient of a pre-doctoral FPI fellowship from the Spanish Education and Sciences Ministry.

## References

- Glucksmann A (1951) Cell deaths in normal vertebrate ontogeny. *Biol Rev Camb Philos Soc* 26:59–86
- Zakeri ZF, Ahuja HS (1994) Apoptotic cell death in the limb and its relationship to pattern formation. *Biochem Cell Biol* 72:603–613
- Zuzarte-Luis V, Hurlle JM (2005) Programmed cell death in the embryonic vertebrate limb. *Semin Cell Dev Biol* 16:261–269
- Merino R, Rodríguez-Leon J, Macías D, Ganan Y, Economides AN, Hurlle JM (1999) The BMP antagonist gremlin regulates outgrowth, chondrogenesis and programmed cell death in the developing limb. *Development* 126:5515–5522
- Fallon JF, Cameron J (1977) Interdigital cell death during limb development of the turtle and lizard with an interpretation of evolutionary significance. *J Embryol Exp Morphol* 40:285–289
- Weatherbee SD, Behringer RR, Rasweiler JJ 4th, Niswander LA (2006) Interdigital webbing retention in bat wings illustrates genetic changes underlying amniote limb diversification. *Proc Natl Acad Sci USA* 103:15103–15107
- Garcia-Martinez V, Macías D, Ganan Y, Garcia-Lobo JM, Francia MV, Fernandez-Teran MA, Hurlle JM (1993) Internucleosomal DNA fragmentation and programmed cell death (apoptosis) in the interdigital tissue of the embryonic chick leg bud. *J Cell Sci* 106:201–208
- Zakeri ZF, Quaglini D, Latham T, Lockshin RA (1993) Delayed internucleosomal DNA fragmentation in programmed cell death. *FASEB J* 7:470–478
- Hurlle J, Hinchcliffe JR (1978) Cell death in the posterior necrotic zone (PNZ) of the chick wing-bud: a stereoscan and ultrastructural survey of autolysis and cell fragmentation. *J Embryol Exp Morphol* 43:123–136
- Hurlle JM, Ros MA, Climent V, Garcia-Martinez V (1996) Morphology and significance of programmed cell death in the developing limb bud of the vertebrate embryo. *Microsc Res Tech* 34:236–246
- Lindsten T, Ross AJ, King A, Zong WX, Rathmell JC, Shiels HA, Ulrich E, Waymire KG, Mahar P, Frauwirth K et al (2000) The combined functions of proapoptotic Bcl-2 family members Bak and Bax are essential for normal development of multiple tissues. *Mol Cell* 6:1389–1399
- Hutcheson J, Scatizzi JC, Bickel E, Brown NJ, Bouillet P, Strasser A, Perlman H (2005) Combined loss of proapoptotic genes Bak or Bax with Bim synergizes to cause defects in hematopoiesis and in thymocyte apoptosis. *J Exp Med* 201:1949–1960
- Boya P, Kroemer G (2008) Lysosomal membrane permeabilization in cell death. *Oncogene* 27:6434–6451
- Zhang H, Zhong C, Shi L, Guo Y, Fan Z (2009) Granulysin induces cathepsin B release from lysosomes of target tumor cells to attack mitochondria through processing of bid leading to necroptosis. *J Immunol* 182:6993–7000
- Castino R, Bellio N, Nicotra G, Follo C, Trincerri NF, Isidoro C (2007) Cathepsin D-Bax death pathway in oxidative stressed neuroblastoma cells. *Free Radic Biol Med* 42:1305–1316
- Zuzarte-Luis V, Berciano MT, Lafarga M, Hurlle JM (2006) Caspase redundancy and release of mitochondrial apoptotic factors characterize interdigital apoptosis. *Apoptosis* 11:701–715
- Wang J, Lenardo MJ (2000) Roles of caspases in apoptosis, development, and cytokine maturation revealed by homozygous gene deficiencies. *J Cell Sci* 113:753–757
- Zuzarte-Luis V, Montero JA, Kawakami Y, Izpisua-Belmonte JC, Hurlle JM (2007) Lysosomal cathepsins in embryonic programmed cell death. *Dev Biol* 301:205–217
- Chautan M, Chazal G, Cecconi F, Gruss P, Golstein P (1999) Interdigital cell death can occur through a necrotic and caspase-independent pathway. *Curr Biol* 9:967–970
- Nagasaka A, Kawane K, Yoshida H, Nagata S (2009) Apaf-1-independent programmed cell death in mouse development. *Cell Death Differ* 17:931–941
- Stewart S, Yi S, Kassabian G, Mayo M, Sank A, Shuler C (2000) Changes in expression of the lysosomal membrane glycoprotein, LAMP-1 in interdigital regions during embryonic mouse limb development, in vivo and in vitro. *Anat Embryol (Berl)* 201:483–490
- Salas-Vidal E, Lomeli H, Castro-Obregon S, Cuervo R, Escalante-Alcalde D, Covarrubias L (1998) Reactive oxygen species participate in the control of mouse embryonic cell death. *Exp Cell Res* 238:136–147
- Schnabel D, Salas-Vidal E, Narvaez V, Sanchez-Carbente Mdel R, Hernandez-Garcia D, Cuervo R, Covarrubias L (2006) Expression and regulation of antioxidant enzymes in the developing limb support a function of ROS in interdigital cell death. *Dev Biol* 291:291–299
- Liu X, Zou H, Slaughter C, Wang X (1997) DFF, a heterodimeric protein that functions downstream of caspase-3 to trigger DNA fragmentation during apoptosis. *Cell* 89:175–184
- Counis MF, Torriglia A (2006) Acid DNases and their interest among apoptotic endonucleases. *Biochimie* 88:1851–1858
- McIlroy D, Tanaka M, Sakahira H, Fukuyama H, Suzuki M, Yamamura K, Ohsawa Y, Uchiyama Y, Nagata S (2000) An auxiliary mode of apoptotic DNA fragmentation provided by phagocytes. *Genes Dev* 14:549–558
- Krieser RJ, MacLea KS, Longnecker DS, Fields JL, Fiering S, Eastman A (2002) Deoxyribonuclease IIalpha is required during the phagocytic phase of apoptosis and its loss causes perinatal lethality. *Cell Death Differ* 9:956–962

28. Kawane K, Nagata S (2008) Nucleases in programmed cell death. *Methods Enzymol* 442:271–287
29. Ros MA, Rivero FB, Hinchliffe JR, Hurle JM (1995) Immunohistological and ultrastructural study of the developing tendons of the avian foot. *Anat Embryol (Berl)* 192:483–496
30. Hurle JM, Kitten GT, Sakai LY, Volpin D, Solursh M (1994) Elastic extracellular matrix of the embryonic chick heart: an immunohistological study using laser confocal microscopy. *Dev Dyn* 200:321–332
31. Hamburger V, Hamilton HL (1992) A series of normal stages in the development of the chick embryo 1951. *Dev Dyn* 195:231–272
32. Padron-Barthe L, Courta J, Lepretre C, Nagbou A, Torriglia A (2008) Leukocyte elastase inhibitor, the precursor of L-DNase II, inhibits apoptosis by interfering with caspase-8 activation. *Biochim Biophys Acta* 1783:1755–1766
33. MacLea KS, Cheng HH (2006) Cloning and expression of deoxyribonuclease II from chicken. *Gene* 373:44–51
34. Padron-Barthe L, Lepretre C, Martin E, Counis MF, Torriglia A (2007) Conformational modification of serpins transforms leukocyte elastase inhibitor into an endonuclease involved in apoptosis. *Mol Cell Biol* 27:4028–4036
35. Livak KJ, Schmittgen TD (2001) Analysis of relative gene expression data using real-time quantitative PCR and the  $2^{-\Delta\Delta C_t}$  method. *Methods* 25:402–408
36. Weil M, Jacobson MD, Coles HS, Davies TJ, Gardner RL, Raff KD, Raff MC (1996) Constitutive expression of the machinery for programmed cell death. *J Cell Biol* 133:1053–1059
37. Hitomi J, Christofferson DE, Ng A, Yao J, Degtarev A, Xavier RJ, Yuan J (2008) Identification of a molecular signaling network that regulates a cellular necrotic cell death pathway. *Cell* 135:1311–1323
38. Torriglia A, Lepretre C, Padron-Barthe L, Chahory S, Martin E (2008) Molecular mechanism of L-DNase II activation and function as a molecular switch in apoptosis. *Biochem Pharmacol* 76:1490–1502
39. Guillemot FP, Oliver PD, Peault BM, Le Douarin NM (1984) Cells expressing Ia antigens in the avian thymus. *J Exp Med* 160:1803–1819
40. Torriglia A, Perani P, Brossas JY, Altairac S, Zeggai S, Martin E, Treton J, Courtois Y, Counis MF (2000) A caspase-independent cell clearance program. the LEI/L-DNase II pathway. *Ann N Y Acad Sci* 926:192–203
41. Hernandez-Martinez R, Castro-Obregon S, Covarrubias L (2009) Progressive interdigital cell death: regulation by the antagonistic interaction between fibroblast growth factor 8 and retinoic acid. *Development* 136:3669–3678
42. Galluzzi L, Vicencio JM, Kepp O, Tasdemir E, Maiuri MC, Kroemer G (2008) To die or not to die: that is the autophagic question. *Curr Mol Med* 8:78–91
43. Hurle JM, Colvee E, Fernandez-Teran MA (1985) Vascular regression during the formation of the free digits in the avian limb bud: a comparative study in chick and duck embryos. *J Embryol Exp Morphol* 85:239–250
44. Erdal H, Berndtsson M, Castro J, Brunk U, Shoshan MC, Linder S (2005) Induction of lysosomal membrane permeabilization by compounds that activate p53-independent apoptosis. *Proc Natl Acad Sci USA* 102:192–197
45. He C, Klionsky DJ (2009) Regulation mechanisms and signaling pathways of autophagy. *Annu Rev Genet* 43:67–93
46. Mizushima N, Yoshimori T, Levine B (2010) Methods in mammalian autophagy research. *Cell* 140:313–326
47. Bass BP, Tanner EA, Mateos San Martin D, Blute T, Kinser RD, Dolph PJ, McCall K (2009) Cell-autonomous requirement for DNaseII in nonapoptotic cell death. *Cell Death Differ* 16:1362–1371
48. Hurle JM, Fernandez-Teran MA (1984) Fine structure of the interdigital membranes during the morphogenesis of the digits of the webbed foot of the duck embryo. *J Embryol Exp Morphol* 79:201–210
49. Montero JA, Hurle JM (2009) Sculpturing digit shape by cell death. *Apoptosis* 15:365–375
50. Hurle JM, Fernandez-Teran MA (1983) Fine structure of the regressing interdigital membranes during the formation of the digits of the chick embryo leg bud. *J Embryol Exp Morphol* 78:195–209
51. Hurle JM, Corson G, Daniels K, Reiter RS, Sakai LY, Solursh M (1994) Elastin exhibits a distinctive temporal and spatial pattern of distribution in the developing chick limb in association with the establishment of the cartilaginous skeleton. *J Cell Sci* 107:2623–2634
52. Nakanishi K, Maruyama M, Shibata T, Morishima N (2001) Identification of a caspase-9 substrate and detection of its cleavage in programmed cell death during mouse development. *J Biol Chem* 276:41237–41244
53. Bergeron L, Perez GI, Macdonald G, Shi L, Sun Y, Jurisicova A, Varmuza S, Latham KE, Flaws JA, Salter JC et al (1998) Defects in regulation of apoptosis in caspase-2-deficient mice. *Genes Dev* 12:1304–1314
54. Kuida K, Haydar TF, Kuan CY, Gu Y, Taya C, Karasuyama H, Su MS, Rakic P, Flavell RA (1998) Reduced apoptosis and cytochrome *c*-mediated caspase activation in mice lacking caspase 9. *Cell* 94:325–337
55. Torriglia A, Lepretre C (2009) LEI/L-DNase II: interplay between caspase-dependent and independent pathways. *Front Biosci* 14:4836–4847
56. MacLea KS, Krieser RJ, Eastman A (2003) A family history of deoxyribonuclease ii: surprises from *Trichinella Spiralis* and *Burkholderia Pseudomallei*. *Gene* 305:1–12
57. Nakahara M, Nagasaka A, Koike M, Uchida K, Kawane K, Uchiyama Y, Nagata S (2007) Degradation of nuclear DNA by DNase II-like acid DNase in cortical fiber cells of mouse eye lens. *FEBS J* 274:3055–3064
58. Wood W, Turmaine M, Weber R, Camp V, Maki RA, McKercher SR, Martin P (2000) Mesenchymal cells engulf and clear apoptotic footplate cells in macrophageless PU.1 null mouse embryos. *Development* 127:5245–5252
59. Milligan CE, Prevette D, Yaginuma H, Homma S, Cardwell C, Fritz LC, Tomaselli KJ, Oppenheim RW, Schwartz LM (1995) Peptide inhibitors of the ICE protease family arrest programmed cell death of motoneurons in vivo and in vitro. *Neuron* 15:385–393